



1 Biogeochemical processes accounting for the natural mercury 2 variations in the Southern Ocean diatom ooze sediments

3 Sara Zaferani¹, Harald Biester¹

4 ¹Institut für Geoökologie AG Umweltgeochemie, Technische Universität Braunschweig, Braunschweig, 38106, Germany

5 *Correspondence to:* Sara Zaferani (s.zaferani@tu-braunschweig.de)

6 **Abstract.** Understanding the marine biogeochemical cycle of mercury is crucial as consumption of mercury enriched marine
7 fish is the most important pathway of mercury uptake by humans. However, due to the lack of long term marine records, the
8 role of the oceans in the global mercury cycle is poorly understood and we do not have well documented data of natural
9 mercury accumulations during changing environmental conditions, e.g. sea surface conditions in the ocean. To understand
10 influence of different sea surface conditions (climate induced changes in ice coverage and biological production) on natural
11 mercury accumulation, we used a continuous ~ 170 m Holocene biogenic sedimentary record from Adélie Basin, East
12 Antarctica, which mainly consists of silica based skeletons of diatoms. We performed Principal Component Analysis and
13 regression analysis on element concentrations and corresponding residual of element concentrations, respectively to investigate
14 the link between sediment mercury accumulation, terrestrial inputs, and productivity. Preindustrial mercury accumulation in
15 the remote pristine marine Antarctica showed extremely high accumulation rates (median: 556 $\mu\text{g m}^{-2} \text{yr}^{-1}$) that displayed
16 periodic-like variations. Our analysis shows that the variations in total mercury concentrations and accumulation rates are
17 associated with biological production and related scavenging of available water phase mercury by rapidly sinking algae or
18 algae derived organic matter after intense algae blooms. High accumulation rates of other studied elements further revealed
19 that in regions of high primary productivity, settling of biogenic materials removes many other elements from ocean surface
20 (through scavenging or biological uptake). In conclusion, the link between mercury cycling and primary production will need
21 to be considered in future studies of the marine mercury cycle under future primary production enhancement through climatic,
22 temperature, and nutrient availability changes.

23 1 Introduction

24 Mercury (Hg) is a metal of environmental concern due to its ability to be transported from source to background regions
25 (predominantly in the atmosphere) and be transformed into highly bioaccumulative and toxic methylated forms. In the
26 biogeochemical cycle of Hg, the ocean, as the dominant physical feature of our planet Earth, is of specific concern. A



27 substantial amount of Hg (~ 80 %) which is emitted to the atmosphere from natural and anthropogenic sources reaches the
28 ocean (Horowitz et al., 2017; Schartup et al., 2019) and ocean sediments have been considered as an ultimate sink of Hg on a
29 timescale of tens of thousands of years (Fitzgerald et al., 2007; Selin, 2009; Amos et al., 2013). Despite the critical role this
30 sink process plays in the Hg biogeochemical cycle, little is known about the rates or amount of Hg accumulation in marine
31 sediments, especially in the open ocean. In contrast to the well studied Hg cycling in terrestrial environments knowledge about
32 the temporal and spatial distribution of Hg in the marine environment is limited to model estimations (Mason and Sheu, 2002;
33 Sunderland and Mason, 2007) and water column measurements (Cossa et al., 2011; Lamborg et al., 2014). A main reason for
34 our limited understanding of the fate of Hg in the oceans is the lack of high resolution marine sedimentary records, especially
35 from the deep ocean (Zaferani et al., 2018).

36 The Hg input to the ocean is primarily through atmospheric deposition (Mason et al., 1994; Driscoll et al., 2013). After
37 deposition, as either mercuric ion (Hg^{2+}) or elemental Hg (Hg^0), Hg can be (i) reduced to Hg^0 and evaded to the atmosphere,
38 or (ii) scavenged from the water column by particulate matter and eventually buried in deep sea sediments, or (iii) methylated
39 to either monomethylmercury (CH_3Hg^+) or dimethylmercury ($(\text{CH}_3)_2\text{Hg}$) (Mason et al., 2012; Lamborg et al., 2014). While
40 models may differ in their predicted Hg values in the surface, subsurface and deep ocean, they all agree that the flux of Hg to
41 the deep ocean is low (Lamborg et al., 2002; Mason and Sheu, 2002; Sunderland and Mason, 2007; Amos et al., 2013). Mason
42 and Sheu (2002) estimated that almost 96 % of the atmospheric Hg flux to the ocean is lost through re-emission from the ocean
43 surface and only 30 % of the Hg flux that reaches the deep ocean is preserved in sediments. However, available data sets on
44 Hg fluxes to deep oceans and accumulation rates in deep ocean sediments are limited and applying the model estimations
45 across the entire ocean introduces substantial uncertainty.

46 One area in particular that highlights this uncertainty is the underestimation of the role of biological productivity in the global
47 Hg cycle. The marine biogeochemical cycle of many elements (Morel and Price, 2003), including Hg (Lamborg et al., 2016;
48 Zaferani et al., 2018), in seawater is controlled directly and indirectly by biological productivity. Regions of high biological
49 productivity play an important role in the downward transport and burial of biologically essential and nonessential elements
50 in the sediments of the deep sea (Schlesinger and Bernhardt, 2013). This assumption for Hg is supported by water column
51 measurements. Lamborg et al. (2014) showed a nutrient like distribution of Hg in the water column of oceans. This study
52 indicates that similar to carbon (C) and phosphorus, Hg shows higher concentrations in the deep water due to its release during
53 organic matter decomposition. This can be due to the Hg—phytoplankton interactions and taking up of Hg from the water
54 phase by phytoplankton (Le Faucheur et al., 2014; Mason et al., 1996). This interaction controls the flux of Hg from the water
55 column to sediments in several ways. First, scavenging of Hg from surface water by particulate organic matter reduces the
56 availability of Hg^{2+} for reduction to Hg^0 . So, the re-emission flux of Hg^0 from productive regions will be lower (Soerensen et
57 al., 2016; Zaferani et al., 2018). Second, Hg scavenging by algae removes Hg from the dissolved phase and may shift the flux



58 of Hg between the atmosphere and the ocean towards the dissolved phase by changing the dissolution equilibrium (Biester et
59 al., 2018; Zaferani et al., 2018). Third, removal of dissolved Hg from the water column by algae and other particulate matter
60 facilitates the downward flux of Hg to the seafloor (Lamborg et al., 2016), which, as mentioned, has traditionally been
61 considered to be slow in its nature. Thus, underestimating the role of biological productivity in the marine biogeochemical
62 cycle of Hg may lead to an overestimation of re-emission fluxes from surface water and underestimates the Hg flux to deep
63 sea sediments.

64 In this context, the Southern Ocean is of particular interest due to its high concentrations of nutrients and related elevated
65 primary productivity (Arrigo et al., 1998). In the Southern Ocean, diatoms are major primary producers (Crosta et al., 2005).
66 Their siliceous cell walls preserve well in sediments and form diatom ooze (Fütterer, 2006). The sedimentation rate of diatom
67 ooze is estimated to reach up to 2 cm yr⁻¹ (Escutia et al., 2011). This high sedimentation rate makes diatom ooze deposits
68 around Antarctica a unique geochemical archive to study the influence of primary productivity on the accumulation of Hg as
69 well as to entangle changes in the natural and anthropogenic marine biogeochemical cycle.

70 Despite providing a unique geochemical archive, studies on Hg cycling in the Southern Ocean and particularly in the Antarctic
71 region are generally limited to the water column (Cossa et al., 2011) and ice cores measurements (Vandal et al., 1993). Cossa
72 et al. (2011) showed that Hg concentrations range between 0.63 and 2.76 pmol L⁻¹ in open water, 1.15 ± 0.22 pmol L⁻¹ in
73 Antarctic Intermediate Water, and 1.35 ± 0.39 pmol L⁻¹ in Antarctic Bottom Water between the Antarctic continent and
74 Tasmania. The observed variations in the vertical distributions of Hg were attributed to air-sea exchange and the affinity of
75 Hg to bind to planktonic and inorganic particulate matter in the biologically productive zone. Hg concentrations in an ice core,
76 covering the past 34 Kyr, varied between 0.0005 and 0.0021 µg kg⁻¹, corresponding to depositional fluxes of 0.009 and 0.031
77 µg m⁻² yr⁻¹ during the Holocene and the Last Glacial Maximum, respectively (Vandal et al., 1993). Vandal et al. (1993)
78 attributed the observed enhanced Hg flux during colder periods to marine biological productivity and emissions of volatile Hg
79 compounds from the ocean.

80 In a previous paper, we discussed the accumulation of anthropogenic Hg in Adélie Basin sediments. The ~ 2-fold increase in
81 Hg concentrations and accumulation rates in the upper ~ 2.80 m depth of the core was attributed to the onset of the industrial
82 revolution and the strong increase in coal burning at ~ 1850 CE (Zaferani et al., 2018). Here we discuss the natural processes
83 (e.g. changes in biogenic and terrestrial material fluxes) that controlled Hg accumulation in the same sediment core prior to
84 1850 CE throughout the past 8600 years. We investigated the continuous ~ 170 m long Holocene laminated diatom ooze
85 sediment record from Adélie Basin offshore East Antarctica. Covering almost the entire Holocene, the core allows the
86 determination of natural variations in Hg accumulation rates in these sediments prior to major anthropogenic influences. Our
87 main objective was to investigate the influence of different Hg sources, climate induced changes in biological productivity and



88 terrestrial fluxes (through melting of glacier ice), which have controlled the sequestration of Hg in these sediments. To evaluate
89 the influence of different biogeochemical processes on the Hg accumulation in sediments, with an emphasis on the role of
90 changes in planktonic productivity, we combined the data on Hg accumulation with data derived from multi element analyses.

91 **2. Materials and methods**

92 **2.1 Study site and core collection**

93 Sediments of the Adélie Basin were collected during the Integrated Ocean Drilling Program (IODP) Expedition from the hole
94 U1357B 318 in 2010. The hole U1357B is located on the continental shelf off Wilkes Land at the Mertz Glacier polynya
95 (regions of open water surrounded by sea ice), Antarctica (66°24.7990' S, 140°25.5705' E) at about 1021.5 m water depth
96 (Escutia et al., 2011) (Fig 1). The total length of the recovered core is 170.7 m, corresponding to nearly the entire Holocene
97 (Escutia et al., 2011). The core was sliced by 5cc plastic scoops (1cm wide samples). Samples in the upper core (3.2–25.05
98 mbsf) were taken at a resolution of ~ 20 years and at resolutions of ~ 200 years in deeper sections (25.05–170.35 mbsf),
99 resulting in a total of 78 samples.

100 The sediment core is characterized by light and dark laminations which are undisturbed by sea level changes or glacial erosion
101 (Denis et al., 2006; Escutia et al., 2011). Light laminations correspond to spring seasons when light and high nutrients levels
102 promote intense phytoplankton blooms and are mainly composed of biogenic materials, i.e. mostly diatom with minor
103 abundance of silicoflagellates, sponge spicules, radiolarians, and foraminifers. Whereas dark layers correspond to the
104 summer/autumn season when sea ice has retreated, and nutrient levels are low. Dark laminations are composed of a mixture
105 of biogenic and terrigenous materials resulting from summer production in open water and glacial and subglacial inputs,
106 respectively. High levels of primary production in surface water of this region coupled with rapid fluxes of biogenic debris,
107 directly to the seafloor, led to high sedimentation rates of up to 2.0 cm yr⁻¹ during the past 10,000 years (Escutia et al., 2011).

108 **2.2 Analyses of mercury and major and trace metals**

109 All samples were freeze dried and ground using a glass pestle prior to geochemical analysis. Total Hg was determined by
110 thermal decomposition followed by pre-concentration of Hg on a gold trap and CVAAS Hg detection using a Milestone DMA-
111 80 analyzer (US EPA Method 1998). The quality of the analysis was ensured by including a certified reference material (CRM)
112 (Canmet LKSD-4 = 190 ± 17 ng g⁻¹) alongside the analyzed samples. The average measured concentration for LKSD-4 was
113 197 ± 11 ng g⁻¹. Replicate analyses (n = 20) were always within an RSD of 10 % of the certified value.

114 The samples were analyzed for concentrations of silicon (Si), titanium (Ti), zirconium (Zr), sulfur (S), calcium (Ca), potassium
115 (K), aluminum (Al), yttrium (Y), manganese (Mn), strontium (Sr), iron (Fe), lead (Pb), copper (Cu), zinc (Zn), arsenic (As),



116 bromine (Br), nickel (Ni), chlorine (Cl), and rubidium (Rb) by means of energy dispersive X-ray fluorescence (ED-XRF). The
117 calibration method, accuracy, and precision are described in detail in Cheburkin and Shotyk (1996). The CRMs (Canmet
118 LKSD-4, NRC/CNRC-PACS-2, NRC/CNR-Mess-3, and NCS-DC75304) and replicates were measured in each set of samples
119 for accuracy and precision control. Repeated analysis of CRMs gave relative standard deviation (SRD) less than 10 % for Si,
120 Al, Ca, Y, Sr, Zr, Br, and Rb, 6–15 % for Ti, K, Zn, S, Fe, Mn, and Pb, 6–19 % for Cl, 10–20 % for Ni, 9–14 % for Cu, and
121 14–22 % for As.

122 **2.3 Statistical analyses**

123 Principal component analysis (PCA) was applied to the major and trace element concentrations to identify processes
124 controlling the variability of elements in the sediments. When there is a complex set of variables, PCA is used to reduce a large
125 number of variables to a new set of artificial variables, called principal components. Each component includes variables with
126 a similar down core pattern. The principal components are then interpreted in terms of relevant geochemical processes that can
127 control the variability of the major and trace elements in the sediments. The derived interpretation from PCA was then
128 combined with the Hg data to examine the processes that could affect Hg accumulations. The analysis was performed on the
129 standardized concentration data using Z-scores.

130 Regressions analysis of the corresponding residuals was used, too to establish the important elemental relationships, by
131 considering Si concentration as an independent variable and other element concentrations as dependent variables. Correlation
132 analysis and PCA were performed using the statistical software SPSS 25.0.

133 **3. Results and discussion**

134 **3.1 Elemental composition of the diatom ooze sediments and geochemical processes controlling their distribution**

135 Concentration profiles and accumulation rates of Si, Al, K, Ti, S, Ca, Zn, Fe, Br, As, and Cl are shown in Fig. 2-5 and discussed
136 in supplementary materials. The preindustrial geochemical record of Adélie Basin sediments is generally characterized by
137 periodic-like variations in the relative abundance of major and trace elements. The records of element accumulation rates
138 largely follow those of periodic-like variations of concentrations and show no significant trend with depth (except Cl).

139 The PCA resulted in five components, explaining almost 82 % of the total variance (Table 1). The first component (Cp1),
140 explains 33 % of the variance and shows large (> 0.7) positive loadings of Mn, Ti, Rb, Zr, K, and Y and moderate positive
141 loading of Fe. The second component (Cp2), which explains 20 % of the variance, is characterized by large positive loadings
142 of Al, Si, S, and Cl and moderate positive loading of K and Ca. The third component (Cp3) explains 17 % of the variance and
143 shows large positive loadings of Zn, Cu, and Ni and moderate positive loading of Fe. The fourth and fifth components (Cp4



144 and Cp5) account for 7 and 5 % of the variance, respectively. Cp4 is characterized by high positive loadings for Hg and As
145 and moderate negative loading of Pb. Cp5 shows positive loadings for Sr and Ca.

146 In general, results of PCA imply that opening and closing of the polynya and biological production are the most important
147 factors influencing sedimentation in Adélie Basin. This has been shown by loadings of elemental proxies for terrigenous and
148 biological material inputs. Briefly, Cp1, which includes positive loadings of lithogenic elements, represents the variability of
149 terrigenous inputs. Melting of ice releases trapped lithogenic material into the water and leads to the sinking of lithogenic
150 particles and their sedimentation. Cp2 comprises loading of elements of both biogenic and terrigenous sources. This component
151 appears to reflect phytoplankton blooms and export of biological materials. After ice melt, when the ice is opening, favorable
152 conditions for biological productivity lead to phytoplankton blooms and export of biogenic materials to the seafloor (Denis et
153 al., 2006). Biogenic material is mainly biogenic silica because diatoms are a major component of blooms in Adélie Basin
154 (Escutia et al., 2011). The sinking of diatoms from the surface and their sedimentation can cause scavenging of elements during
155 bloom time. Al shows positive loadings in this component rather than in Cp1. This, other than association with the flux of
156 aluminosilicates material can also be attributed to the scavenging of Al by diatom particles (Moran and Moore, 1992). Cl also
157 shows loading in Cp2. The possible explanation for the observed covariation is that marine phytoplankton is rich in
158 polyunsaturated lipids and can account as chlorination substrates (Leri et al., 2015). However, the organic C content of Adélie
159 Basin sediments is generally low (between 1 and 2 wt %), and some of the Cl must be in an inorganic form trapped in sediments
160 owing to high sedimentation rates. Cp3 is mainly characterized by elements that are associated with the organic fraction of
161 diatom cells. This component appears to reflect the remineralization process. Trace elements associated with organic parts of
162 cells can be released back into the water column during decomposition. Therefore, cellular locations of elements, i.e. opal
163 frustules of diatoms or organic matter of diatom cells, created different components of Cp2 and Cp3. Cp4 consists of particle
164 reactive metals, e.g. Hg and Pb. The possible explanation for not having these two particle reactive metals in Cp2 is that these
165 two metals begin to enter the system after ice melting, while Cp2 shows scavenging of elements by diatoms that are already
166 present in the water column. Since Pb and Hg are negatively correlated, this component cannot reflect a pollution signal.
167 Covariation of Ca and Sr in Cp5 represents sedimentation of planktonic foraminifera, which appears to be of minor importance
168 here.

169 Cp1 explains 33 % of the variance and accounts for much of the variability/process which controlled the geochemical
170 composition of these sediments. However, the high concentration of Si and low concentrations of terrigenous elements imply
171 that in an environment like Adélie Basin, with extremely high productivity, input of lithogenic materials is changing while
172 different diatoms taxa are always present in the system, e.g. as sea ice associated and open ocean diatom.



173 Although the core was not sampled at one year resolution, the fluctuations of elemental concentrations are likely related to the
174 seasonal variation of sea surface conditions like ice melting and freezing and its subsequent biological or terrestrial materials
175 exports. Sampling in light (associated with spring seasons) or dark (associated with summer/autumn seasons) laminae, which
176 contain different amounts of biogenic or terrestrial materials can cause the observed variations (see Sect. 2.1).

177 The element concentrations are comparable to other published sediment data, while the accumulation rates are much higher
178 than other reported values. The existence of rapidly settling particles in Adélie Basin can explain the high element accumulation
179 rates. The high accumulation rates suggest that most elements in the water column of Adélie Basin are subjected to removal
180 by intense phytoplankton blooms through consumption or scavenging. Aggregation of diatoms, which creates large particles,
181 and their sinking to the seafloor can create a space in which elements can be trapped (Shanks and Trent, 1979). This enhances
182 removal of elements from the water column and their sedimentation as well.

183 3.2 Holocene record of mercury concentrations and accumulation rates

184 In the preindustrial period, i.e. from the bottom of the core at ~ 170 m to 2.80 m depth (8600 years ago to ~ 1850 CE), the Hg
185 record shows no obvious trend with depth but rather periodic-like variations. Hg concentrations fluctuate by a factor of about
186 2 between 12.6 and 21.1 $\mu\text{g kg}^{-1}$ within 170-137 m depth and between 21.7 and 44.6 $\mu\text{g kg}^{-1}$ within 137–2.80 m depth of the
187 core, with two more pronounced peaks at around 9.99 and 8.20 m depth. The lower concentration of Hg within 170-137 m
188 depth of the core is probably attributed to the cooler condition and sea ice cover during this period. Hg accumulation rates in
189 the preindustrial period largely follow the Hg concentration record, with a median of 556 $\mu\text{g m}^{-2} \text{yr}^{-1}$.

190 The high preindustrial Hg accumulation rates in Adélie Basin sediments cannot be explained by preindustrial atmospheric Hg
191 depositions alone, which did not exceed 20 $\mu\text{g m}^{-2}$ as recorded in an Antarctic ice core (Vandal et al., 1993). Therefore, non-
192 atmospheric sources, such as dissolved water phase Hg or terrestrial inputs, are needed for Hg enrichment in these sediments.

193 To identify driving forces behind the variations in Hg accumulation we used our PCA results. PCA demonstrated that two
194 main processes, i.e. biogenic productivity and lithogenic inputs, controlled the flux of elements to Adélie Basin sediments.
195 The component scores, which illustrate the depth dependency of the extracted components, are characterized by see-saw
196 patterns throughout the entire core. This indicates different contributions of biogenic and terrigenous inputs most likely
197 associated with spring and summer/autumn seasons, respectively.

198 The variance of Hg was not captured by Cp1, Cp2 or Cp3. Hg instead forms a group on Cp4 together with positive loading of
199 As and negative loading of Pb. The absence of significant loading of Hg on Cp1, Cp2, and Cp3 (Table 1) and the lack of
200 similarity between component scores and Hg concentrations (Fig. 7 and 8), in the preindustrial period, indicates that Hg fluxes



201 are not significantly influenced by changes in lithogenic inputs through ice melting. These results further indicate that changes
202 in the contribution of biogenic material also do not directly explain the variation of Hg accumulation in the sediments. The
203 main reason for not finding any statistical relation between Hg and biogenic materials is that the amount of algal material
204 during algae blooms is always large and therefore not a limiting factor for the scavenging of Hg. There has always been excess
205 algal material within or passing through the water column to scavenge all water column Hg. Thus, we assume that nearly all
206 Hg in the water column is removed through scavenging during diatom blooms, but that Hg scavenging events do not or less
207 frequently occur during summer/autumn seasons when primary productivity is lower and open ice expansion is at its maximum.
208 Similar to other elements, the periodic-like variations observed in the preindustrial Hg record are likely attributed to the
209 sampling variability at seasonal scales and laminae, which have different content of biogenic and terrestrial materials. This can
210 affect Hg concentrations. However, investigation at seasonal resolution is needed to further confirm our observations.

211 To calculate the amount of Hg which could be at maximum scavenged by a single bloom event we used the Hg concentration
212 of $271 \pm 78 \text{ pg L}^{-1}$ in Antarctic Bottom Water, as suggested by Cossa et al. (2011). A water column of one m^2 and 1000 m
213 depth would then amount to $271 \pm 78 \text{ } \mu\text{g m}^{-2}$. This means that only about 2-3 algae blooms and scavenging events per year are
214 necessary to obtain the average Hg accumulation rate in Adèle Basin diatom ooze sediments, i.e. $556 \pm 137 \text{ } \mu\text{g m}^{-2} \text{ yr}^{-1}$. This
215 appears to be likely taking into account that the sinking speed of diatom agglomerates at Adèle Basin has been reported to
216 reach 100-400 m per day (Jansen et al., 2018). Formation of Antarctic bottom water which is linked to the polynyas (Ohshima
217 et al., 2013) can rapidly “refill” the Hg inventory in the water column after a scavenging event. This calculation suggests the
218 high Hg accumulation rates in the Adèle Basin sediments can be solely explained by scavenging of water column Hg and does
219 not need an additional atmospheric or terrestrial source. Nevertheless, we assume that similar to CO_2 , Hg fluxes from the
220 atmosphere will increase during algae blooms as a result of continuous removal of dissolved phase Hg by diatom particles and
221 the resulting shift of the dissolution equilibrium towards the dissolved phase which should additionally increase the Hg flux
222 from the atmosphere into the water. Hg removal from the upper water phase by diatom organic matter will also decrease Hg
223 re-escape to the atmosphere as previously assumed in a model study (Soerensen et al., 2016).

224 4. Conclusions

225 Investigation of biogenic sediments revealed that biological productivity and related scavenging of water phase Hg by rapidly
226 sinking algae or algae derived organic matter controlled preindustrial Hg accumulation in Adèle Basin, Antarctica. Our study
227 suggests that the periodic-like variations in total Hg concentrations and accumulation rates are likely associated with the cycle
228 of polynya opening and closing and its related changes in biological productivity. Although the high Hg accumulation in
229 diatom ooze does not represent the Hg sedimentation process across all the world’s oceans, our data shows that Hg scavenging
230 by algae or sinking algae derived organic matter is a key process controlling the sequestration of Hg in marine sediments; and



231 therefore the marine biogeochemical cycle of Hg in general. This can be similar to the association between very high benthic
232 organic C fluxes with diatom production at the surface water which can be accelerated by aggregation (Sachs et al., 2009).

233 Our observations also suggest that re-emission of Hg from ocean surface waters as a result of reduction of Hg (II) might be
234 reduced due to Hg scavenging by algae, at least in areas of high primary productivity. Moreover, Hg fluxes to marine sediments
235 might be higher than previously assumed in global model estimations. More data from marine sediments is needed to support
236 this assumption. A future increase in marine productivity including algae blooms especially in coastal areas and semi-closed
237 shallow seas will likely increase the Hg flux to bottom sediments. The model study of Soerensen et al. (2016) for the Baltic
238 Sea might serve as an example for changes in marine Hg cycling caused by eutrophication.

239 *Author contributions.* Sara Zaferani carried out the experiments. Harald Biester encouraged and supervised the findings of this
240 work. All authors contributed to a significant part to the presented scientific work.

241 *Competing interests.* The authors declare that they have no conflict of interest

242 *Acknowledgements.* This research was supported by TU Braunschweig. We thank P. Schmidt and A. Calean for technical
243 assistance, Dr. DS. McLagan for the constructive comments.

244 **References**

245 Amos, H. M., Jacob, D. J., Streets, D. G. and Sunderland, E. M.: Legacy impacts of all-time anthropogenic emissions on the
246 global mercury cycle, *Global Biogeochem. Cycles*, 27, 410–421, <https://doi.org/10.1002/gbc.20040>, 2013.

247 Arrigo, K. R., Worthen, D., Schnell, A. and Lizotte, M. P.: Primary production in Southern Ocean waters, *J. Geophys. Res.*
248 *Ocean.*, 103, 15587–15600, <https://doi.org/10.1029/98JC00930>, 1998.

249 Biester, H., Pérez-Rodríguez, M., Gilfedder, B. S., Martínez Cortizas, A. and Hermanns, Y. M.: Solar irradiance and primary
250 productivity controlled mercury accumulation in sediments of a remote lake in the Southern Hemisphere during the past 4000
251 years, *Limnol. Oceanogr.*, 63, 540–549, <https://doi.org/10.1002/lno.10647>, 2018.

252 Cheburkin, A. K. and Shotyk, W.: An energy-dispersive miniprobe multielement analyzer (EMMA) for direct analysis of Pb
253 and other trace elements in peats, *Fresenius. J. Anal. Chem.*, 354, 688–691, <https://doi.org/10.1007/s0021663540688>, 1996.

254 Chen, S.-Y., Ambe, S., Takematsu, N. and Ambe, F.: The chemical states of iron in marine sediments by means of Mössbauer
255 spectroscopy in combination with chemical leachings, *J. Oceanogr.*, 52, 705–715, <https://doi.org/10.1007/BF02239461>, 1996.

256 Cossa, D., Heimbu, L., Lannuzel, D., Rintoul, S. R., Butler, E. C. V., Bowie, A. R., Averty, B., Watson, R. J. and Remenyi, T.:
257 Mercury in the Southern Ocean, *Geochim. Cosmochim. Acta*, 75, 4037–4052, <https://doi.org/10.1016/j.gca.2011.05.001>, 2011.

258 Crosta, X., Romero, O., Armand, L. K. and Pichon, J.-J.: The biogeography of major diatom taxa in Southern Ocean sediments:
259 2. Open ocean related species, *Palaeogeogr. Palaeoclimatol. Palaeoecol.*, 223, 66–92,
260 <https://doi.org/10.1016/j.palaeo.2005.02.015>, 2005.



- 261 Croudace, I. W. and Rothwell, R. G.: Micro-XRF Studies of Sediment Cores: Applications of a non-destructive tool for the
262 environmental sciences, Springer., 2015.
- 263 Denis, D., Crosta, X., Zaragosi, S., Romero, O., Martin, B. and Mas, V.: Seasonal and subseasonal climate changes recorded
264 in laminated diatom ooze sediments, Adelie Land, East Antarctica, The Holocene, 16, 1137–1147,
265 <https://doi.org/10.1177%2F0959683606069414>, 2006.
- 266 Driscoll, C. T., Mason, R. P., Chan, H. M., Jacob, D. J. and Pirrone, N.: Mercury as a global pollutant: Sources, pathways, and
267 effects, *Environ. Sci. Technol.*, 47, 4967–4983, <https://doi.org/10.1021/es305071v>, 2013.
- 268 Escutia, C., Brinkhuis, H., Klaus, A. and Scientists, E. 318: Site U1357, *Proc. Integr. Ocean Drill. Programprogr.*, 318,
269 doi:10.2204/iodp.proc.318.105.2011, 2011.
- 270 Le Faucheur, S., Campbell, P. G., Fortin, C. and Slaveykova, V. I.: Interactions between mercury and phytoplankton:
271 speciation, bioavailability, and internal handling, *Environ. Toxicol. Chem.*, 33, 1211–1224, <https://doi.org/10.1002/etc.2424>,
272 2014.
- 273 Fitzgerald, W. F., Lamborg, C. H. and Hammerschmidt, C. R.: Marine biogeochemical cycling of mercury, *Chem. Rev.*, 107,
274 641–662, <https://doi.org/10.1021/cr050353m>, 2007.
- 275 Fütterer, D. K.: The solid phase of marine sediments, in: *Marine geochemistry*, edited by H. D. Schulz and M. Zabel, pp. 1–
276 25, Springer, Berlin, Heidelberg, https://doi.org/10.1007/978-3-662-04242-7_1%0A, 2006.
- 277 Horowitz, H. M., Jacob, D. J., Zhang, Y., Dibble, T. S., Slemr, F., Amos, H. M., Schmidt, J. A., Corbitt, E. S., Marais, E. A.
278 and Sunderland, E. M.: A new mechanism for atmospheric mercury redox chemistry: implications for the global mercury
279 budget, *Atmos. Chem. Phys.*, 17, 6353–6371, <https://doi.org/10.5194/acp-17-6353-2017>, 2017.
- 280 Jansen, J., Hill, N. A., Dunstan, P. K., McKinlay, J., Sumner, M. D., Post, A. L., Eléaume, M. P., Armand, L. K., Warnock, J.
281 P., Galton-Fenzi, B. K. and Johnson, C. R.: Abundance and richness of key Antarctic seafloor fauna correlates with modelled
282 food availability, *Nat. Ecol. Evol.*, 2, 71–80, <https://doi.org/10.1038/s41559-017-0392-3>, 2018.
- 283 Lamborg, C., Bowman, K., Hammerschmidt, C., Gilmour, C., Munson, K., Selin, N. and Tseng, C.-M.: Mercury in the
284 Anthropocene Ocean, *Oceanography*, 27, 76–87, <https://doi.org/10.5670/oceanog.2014.11>, 2014a.
- 285 Lamborg, C. H., Fitzgerald, W. F., O'Donnell, J. and Torgersen, T.: A non-steady-state compartmental model of global-scale
286 mercury biogeochemistry with interhemispheric atmospheric gradients, *Geochim. Cosmochim. Acta*, 66, 1105–1118,
287 [https://doi.org/10.1016/S0016-7037\(01\)00841-9](https://doi.org/10.1016/S0016-7037(01)00841-9), 2002.
- 288 Lamborg, C. H., Hammerschmidt, C. R., Bowman, K. L., Swarr, G. J., Munson, K. M., Ohnemus, D. C., Lam, P. J.,
289 Heimbürger, L., Rijkenberg, M. J. A. and Saito, M. A.: A global ocean inventory of anthropogenic mercury based on water
290 column measurements, *Nature*, 512, 65–68, <https://doi.org/10.1038/nature13563>, 2014b.
- 291 Lamborg, C. H., Hammerschmidt, C. R. and Bowman, K. L.: An examination of the role of particles in oceanic mercury
292 cycling, *Philos. Trans. R. Soc. A Math. Phys. Eng. Sci.*, 374, 20150297, <https://doi.org/10.1098/rsta.2015.0297>, 2016.
- 293 Leri, A. C., Mayer, L. M., Thornton, K. R., Northrup, P. A., Dunigan, M. R., Ness, K. J. and Gellis, A. B.: A marine sink for
294 chlorine in natural organic matter, *Nat. Geosci.*, 8, 620–624, <https://doi.org/10.1038/ngeo2481>, 2015.

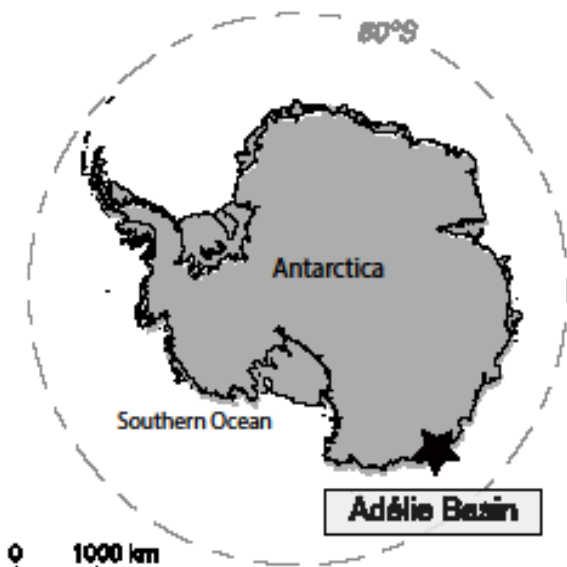


- 295 Lohan, M. C. and Tagliabue, A.: Oceanic micronutrients: trace metals that are essential for marine life, *Elements*, 14, 385–
296 390, <https://doi.org/10.2138/gselements.14.6.385>, 2018.
- 297 Mason, R. and Sheu, G.-R.: Role of the ocean in the global mercury cycle, *Global Biogeochem. Cycles*, 16, 1–14,
298 <https://doi.org/10.1029/2001GB001440>, 2002.
- 299 Mason, R. P., Fitzgerald, W. F. and Morel, F. M.: The biogeochemical cycling of elemental mercury: anthropogenic influences,
300 *Geochim. Cosmochim. Acta*, 58, 3191–3198, [https://doi.org/10.1016/0016-7037\(94\)90046-9](https://doi.org/10.1016/0016-7037(94)90046-9), 1994.
- 301 Mason, R. P., Reinfelder, J. R. and Morel, F. M.: Uptake , Toxicity , and Trophic Transfer of Mercury in a Coastal Diatom,
302 *Environ. Sci. Technol.*, 30, 1835–1845, <https://doi.org/10.1021/es950373d>, 1996.
- 303 Mason, R. P., Choi, A. L., Fitzgerald, W. F., Hammerschmidt, Chad R Lamborg, C. H., Soerensen, A. L. and Sunderland, E.
304 M.: Mercury biogeochemical cycling in the ocean and policy implications, *Environ. Res.*, 119, 101–117,
305 <https://doi.org/10.1016/j.envres.2012.03.013>, 2012.
- 306 Moran, S. and Moore, R.: Kinetics of the removal of dissolved aluminum by diatoms in seawater: A comparison with thorium,
307 *Geochim. Cosmochim. Acta*, 56, 3365–3374, [https://doi.org/10.1016/0016-7037\(92\)90384-U](https://doi.org/10.1016/0016-7037(92)90384-U), 1992.
- 308 Morel, F. M. and Price, N.: The biogeochemical cycles of trace metals in the oceans, *Science*, 300, 944–947,
309 <https://doi.org/10.1126/science.1083545>, 2003.
- 310 Morel, F. M. M., Reinfelder, J. R., Roberts, S. B., Chamberlain, C. P., Lee, J. G. and Yee, D.: Zinc and carbon co-limitation
311 of marine phytoplankton, *Nature*, 369, 740–742, <https://doi.org/10.1038/369740a0>, 1994.
- 312 Ohshima, K. I., Fukamachi, Y., Williams, G. D., Nihashi, S., Roquet, F., Kitade, Y., Tamura, T., Hirano, D., Herraiz-
313 Borreguero, L., Field, I., Hindell, M., Aoki, S. and Wakatsuchi, M.: Antarctic Bottom Water production by intense sea-ice
314 formation in the Cape Darnley polynya, *Nat. Geosci.*, 6, 235–240, <https://doi.org/10.1038/ngeo1738>, 2013.
- 315 Sachs, O., Sauter, E. J., Schlüter, M., Rutgers van der Loeff, M. M., Jerosch, K. and Holby, O.: Benthic organic carbon flux
316 and oxygen penetration reflect different plankton provinces in the Southern Ocean, *Deep. Res. Part I Oceanogr. Res. Pap.*, 56,
317 1319–1335, <https://doi.org/10.1016/j.dsr.2009.02.003>, 2009.
- 318 Schartup, A. T., Thackray, C. P., Qureshi, A., Dassuncao, C., Gillespie, K., Hanke, A. and Sunderland, E. M.: Climate change
319 and overfishing increase neurotoxicant in marine predators, *Nature*, 572, 648–650, <https://doi.org/10.1038/s41586-019-1468-9>, 2019.
- 321 Schlesinger, W. H. and Bernhardt, E. S.: The Oceans, in: *Biogeochemistry: an analysis of global change*, pp. 341–395,
322 Academic press., 2013.
- 323 Selin, N. E.: Global biogeochemical cycling of mercury: a review, *Annu. Rev. Environ. Resour.*, 34, 43–63,
324 <https://doi.org/10.1146/annurev.enviro.051308.084314>, 2009.
- 325 Shanks, A. L. and Trent, J. D.: Marine snow: microscale nutrient patches 1, *Limnol. Oceanogr.*, 24, 850–854,
326 <https://doi.org/10.4319/lo.1979.24.5.0850>, 1979.



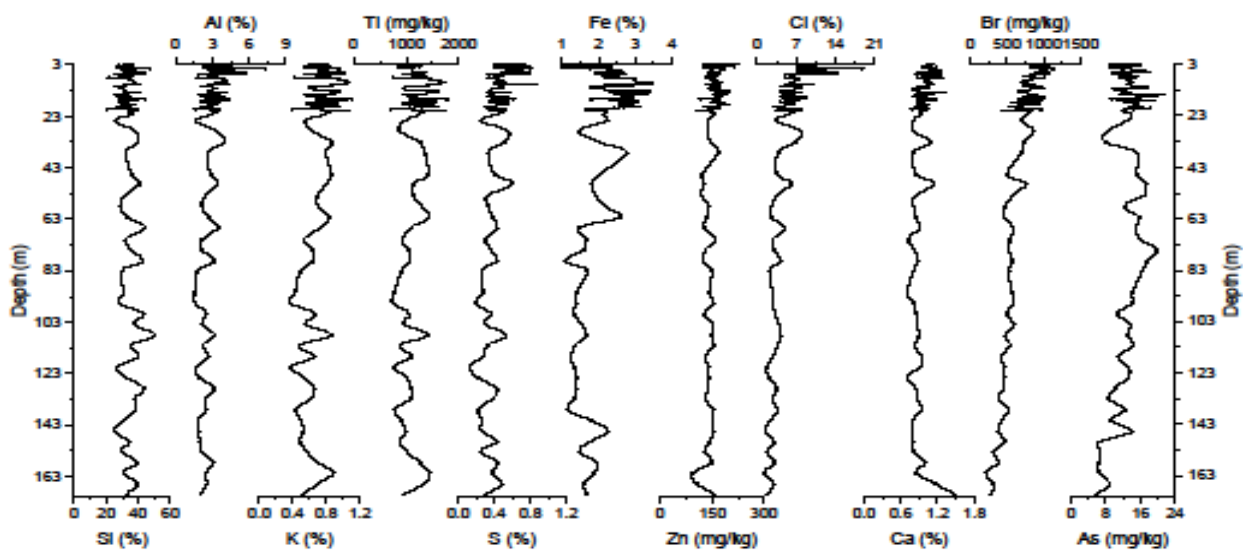
- 327 Soerensen, A. L., Schartup, A. T., Gustafsson, E., Gustafsson, B. G., Undeman, E. and Björn, E.: Eutrophication increases
328 phytoplankton methylmercury concentrations in a coastal sea - A Baltic sea case study, *Environ. Sci. Technol.*, 50, 11787–
329 11796, <https://doi.org/10.1021/acs.est.6b02717>, 2016.
- 330 Sunderland, E. M. and Mason, R. P.: Human impacts on open ocean mercury concentrations, *Global Biogeochem. Cycles*, 21,
331 1–15, <https://doi.org/10.1029/2006GB002876>, 2007.
- 332 Vandal, G. M., Fitzgerald, W. F., Boutron, C. F. and Candelone, J.-P.: Variations in mercury deposition to Antarctica over the
333 past 34,000 years, *Nature*, 362, 621, <https://doi.org/10.1038/362621a0>, 1993.
- 334 Zaferani, S., Pérez-rodríguez, M. and Biester, H.: Diatom ooze—A large marine mercury sink, *Science*, 361, 797–800,
335 <https://doi.org/10.1126/science.aat2735>, 2018.

336



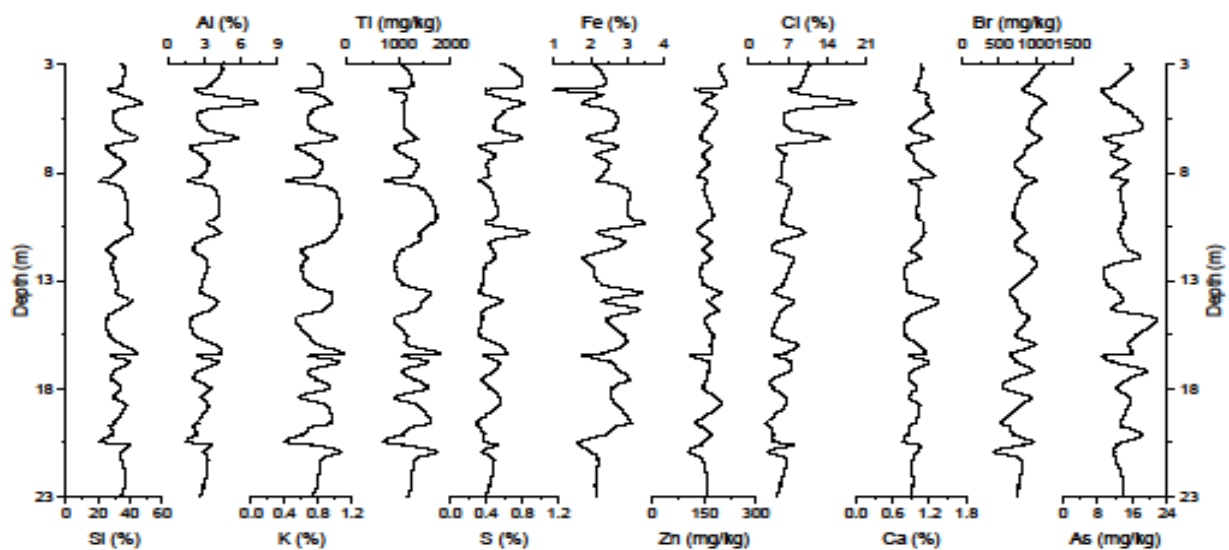
337

338 Figure 1: Map of Antarctica with the coring location of the IODP318-U1357B in Adélie Basin (Source: figure modified from
339 Zaferani et al. (2018)).



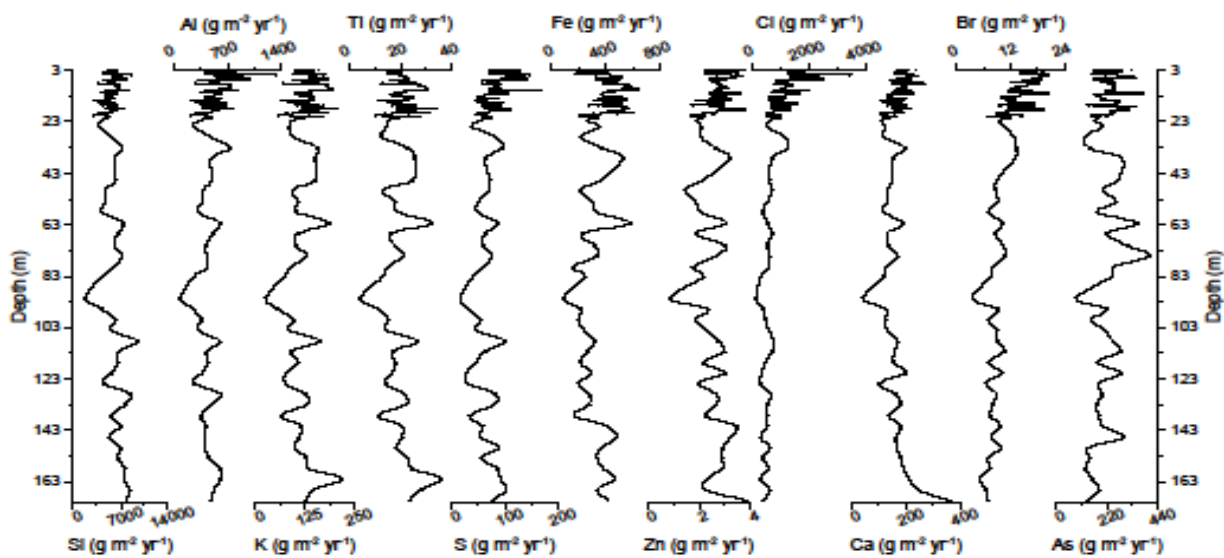
340

341 Figure 2: Down core records of Si, Al, K, Ti, S, Fe, Zn, Cl, Ca, Br, and As concentrations of Adélie Basin sediments.



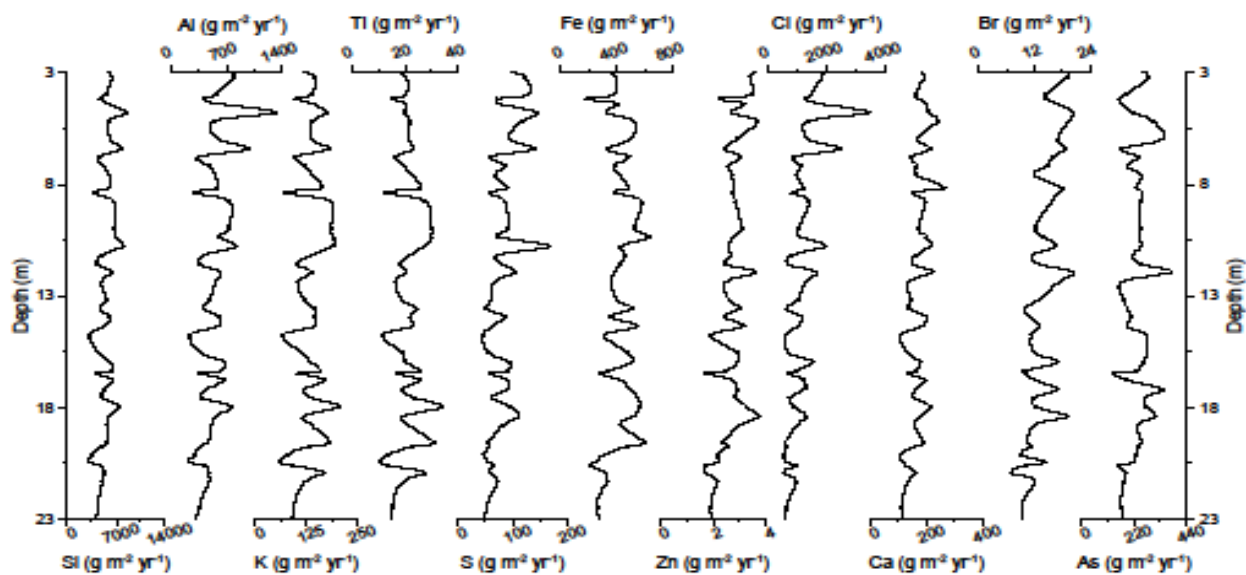
342

343 **Figure 3: Down core records of Si, Al, K, Ti, S, Fe, Zn, Cl, Ca, Br, and As concentrations of Adélie Basin sediments for the top 23 m**
344 **of the core.**



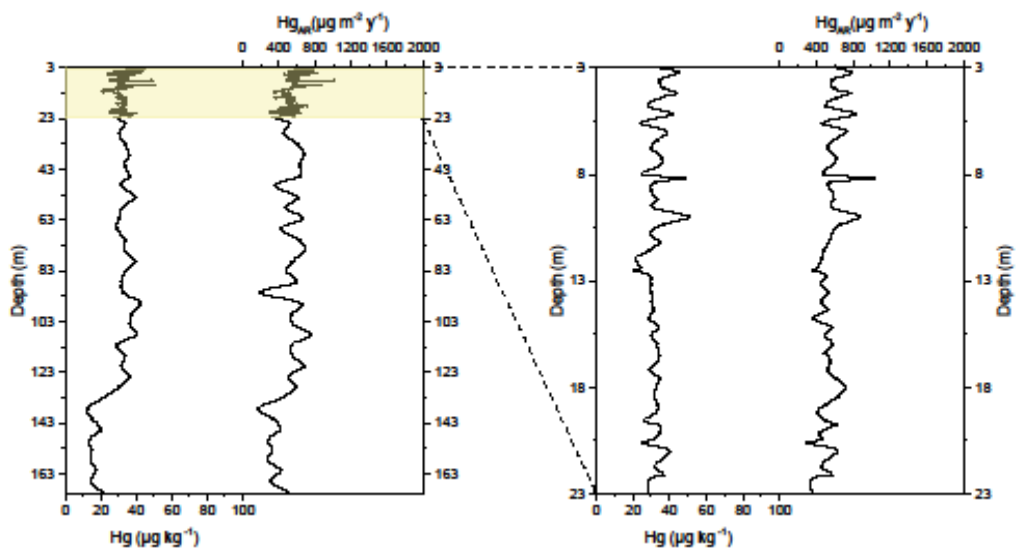
345

346 **Figure 4: Down core records of Si, Al, K, Ti, S, Fe, Zn, Cl, Ca, Br, and As accumulation rates of Adélie Basin sediments.**



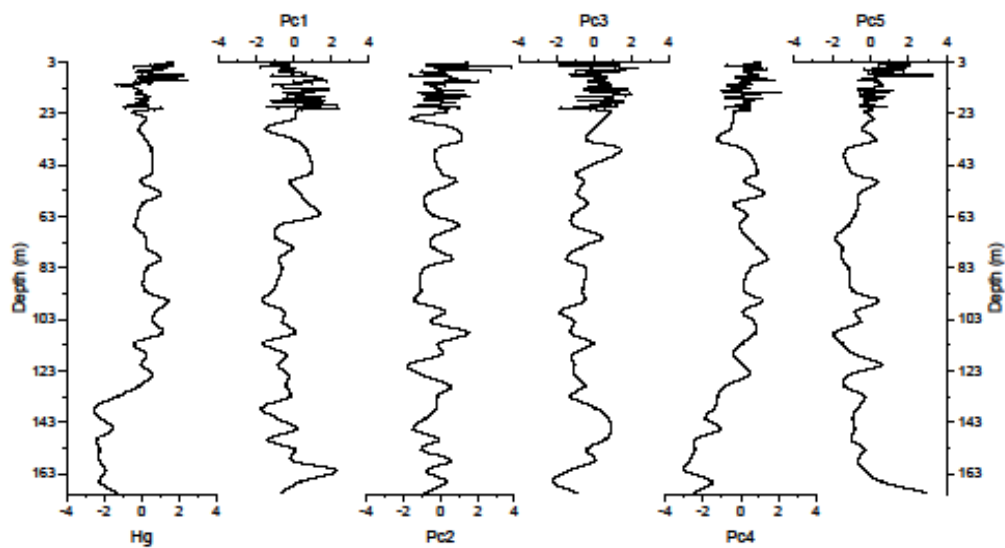
347

348 **Figure 5: Down core records of Si, Al, K, Ti, S, Fe, Zn, Cl, Ca, Br, and As accumulation rates of Adélie Basin sediments for the top**
349 **23 m of the core.**



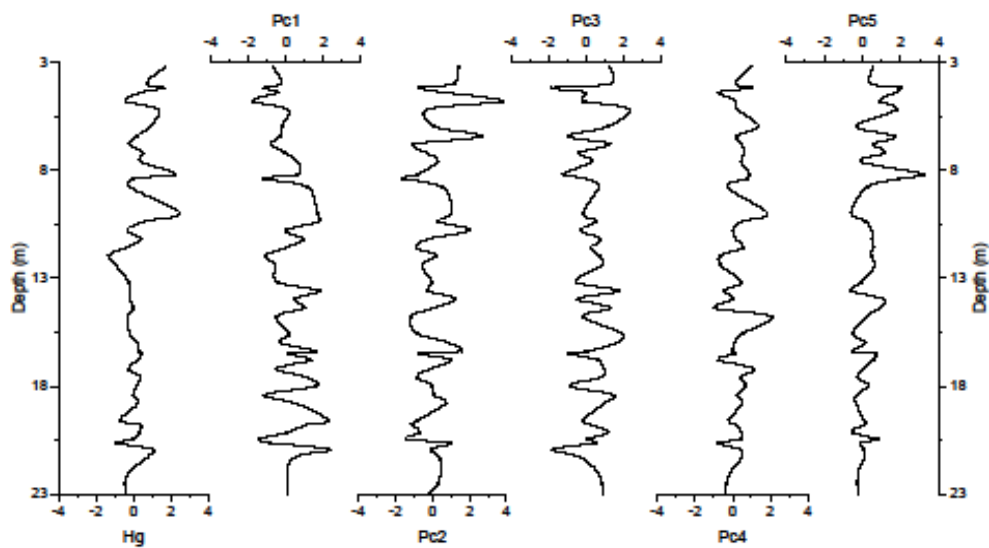
350

351 **Figure 6: Down core records of Hg concentrations and accumulation rates of Adélie Basin sediments.**



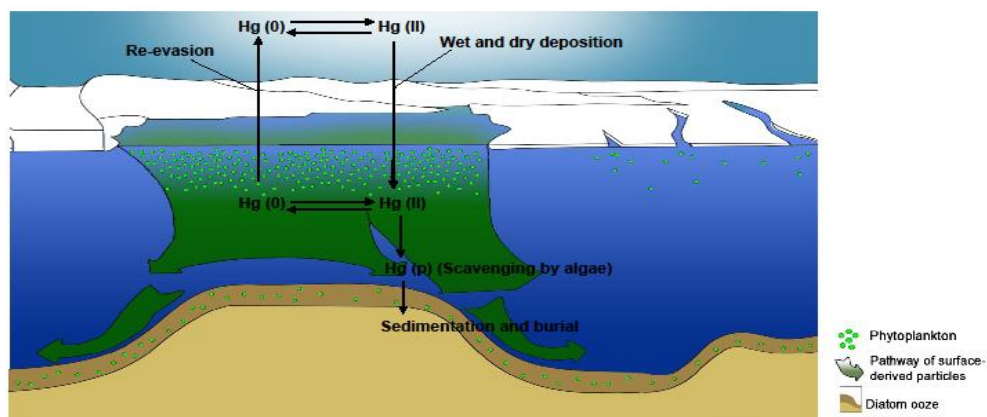
352

353 **Figure 7: Depth records of scores of the principal components extracted by PCA on the elemental composition of the sediments along**
354 **with Z-score of Hg of the Adélie Basin sediments.**



355

356 **Figure 8: Depth records of scores of the principal components extracted by PCA on the elemental composition of the sediments along**
357 **with Z-score of Hg of the Adélie Basin sediments for the top 23 m of the core.**



358

359 **Figure 9: Adélie Basin schematic Hg cycle model indicating the processes controlling Hg deposition and accumulation under high**
360 **primary production. Fast-sinking diatom particles remove dissolved water phase Hg from the water column through scavenging.**
361 **Hg removal from the dissolved phase by diatom particles will also decrease the Hg re-evasion to the atmosphere (Figure is adapted**
362 **from (Jansen et al., 2018).**



363 **Table 1: Factor loadings for the five significant components extracted by PCA from Adélie Basin sediment samples.**

Elements	Components				
	1	2	3	4	5
Mn	0.89	0.40	-0.05	-0.05	0.01
Ti	0.89	0.43	0.01	0.04	-0.02
Rb	0.84	0.03	0.39	0.10	0.20
Zr	0.83	-0.22	0.05	-0.15	0.08
K	0.73	0.66	0.05	0.08	0.10
Y	0.73	-0.34	0.10	-0.09	0.05
Al	0.12	0.93	0.06	0.05	0.18
Si	0.03	0.84	-0.28	-0.11	-0.28
S	0.01	0.84	0.16	0.12	0.26
Cl	-0.16	0.76	0.25	0.22	0.42
Zn	-0.05	0.15	0.78	0.15	0.11
Cu	0.31	0.03	0.76	0.31	0.21
Ni	0.11	-0.08	0.75	-0.10	0.00
Fe	0.62	0.03	0.64	0.20	0.19
Br	-0.23	0.35	0.50	0.46	0.48
Hg	0.17	0.09	-0.04	0.79	0.14
As	-0.01	-0.09	0.30	0.73	-0.26
Pb	0.35	-0.11	-0.10	-0.62	-0.18
Sr	0.25	0.09	0.37	0.16	0.83
Ca	0.22	0.52	-0.03	-0.13	0.67
Eigenvalue	6.62	3.95	3.34	1.35	0.98
% variance	33.1	19.7	16.7	6.7	4.9

364